



Review

# Recent Advances in Vehicle Exhaust Treatment with Photocatalytic Technology

Jianyong Zhao, Jianpeng Sun, Xiangchao Meng  and Zizhen Li \* 

Key Laboratory of Marine Chemistry Theory and Technology, College of Chemistry and Chemical Engineering, Ocean University of China, Ministry of Education, Qingdao 266100, China

\* Correspondence: lizizhen@ouc.edu.cn

**Abstract:** Vehicle exhaust has been acknowledged as an essential factor affecting human health due to the extensive use of cars. Its main components include volatile organic compounds (VOCs) and nitrogen oxides (NO<sub>x</sub>), which can cause acute irritation and chronic diseases, and significant research on the treatment of vehicle exhaust has received increasing attention in recent decades. Recently, photocatalytic technology has been considered a practical approach for eliminating vehicle emissions. This review highlights the crucial role of photocatalytic technology in eliminating vehicle emissions using semiconductor catalysts. A particular emphasis has been placed on various photocatalytic materials, such as TiO<sub>2</sub>-based materials, Bi-based materials, and Metal–Organic Frameworks (MOFs), and their recent advances in the performance of VOC and NO<sub>x</sub> photodegradation. In addition, the applications of photocatalytic technology for the elimination of vehicle exhaust are presented (including photocatalysts combined with pavement surfaces, making photocatalysts into architectural coatings and photoreactors), which will offer a promising strategy for photocatalytic technology to remove vehicle exhaust.

**Keywords:** vehicle exhaust; photocatalysis; photoreactor; volatile organic compounds; nitrogen oxides



**Citation:** Zhao, J.; Sun, J.; Meng, X.; Li, Z. Recent Advances in Vehicle Exhaust Treatment with Photocatalytic Technology. *Catalysts* **2022**, *12*, 1051. <https://doi.org/10.3390/catal12091051>

Academic Editors: Roberto Fiorenza and Jingbo Jia

Received: 19 August 2022

Accepted: 11 September 2022

Published: 15 September 2022

**Publisher's Note:** MDPI stays neutral with regard to jurisdictional claims in published maps and institutional affiliations.



**Copyright:** © 2022 by the authors. Licensee MDPI, Basel, Switzerland. This article is an open access article distributed under the terms and conditions of the Creative Commons Attribution (CC BY) license (<https://creativecommons.org/licenses/by/4.0/>).

## 1. Introduction

Vehicle emissions contain volatile organic compounds (VOCs) and nitrogen oxides (NO<sub>x</sub>), which are the primary sources of air pollution [1–4]. Since their introduction in 1974, three-way catalysts have been continuously improved [5–7]. They have become indispensable for automotive exhaust treatment, and modern vehicles can reduce 99% of toxic emissions for a lifetime of 150,000 km [8]. However, the environment in busy traffic areas severely impacts human health due to the cumulative effect of vehicle emissions from the external environment [9]. The 1% of exhaust gases remaining after the vehicle exhaust system's treatment should be removed.

Many efforts have been applied to developing air purification technologies to address the problem of vehicle exhaust pollution at the source. However, most highly efficient catalysts are modified with precious metals, and the economic cost is too high, which limits their wide application. Moreover, the synthesis methods of some catalysts are too complicated, which hinders their industrial production [10]. Therefore, developing novel technologies, including adsorption [11], plasma [12–15], electrocatalytic oxidation [16], and photocatalytic oxidation, has been proposed to deal with trace amounts of vehicle emissions to reduce the harm of NO<sub>x</sub> and VOCs to human health. Among them, photocatalytic oxidation technology can mineralize VOCs directly into harmless small molecules. It is a better VOC removal technology for low concentrations of different pollutants and even under a low-temperature environment [17–19]. While there are few reviews on photocatalytic technology to eliminate vehicle exhaust, this review focuses on the research and development of photocatalytic oxidation technology for eliminating VOCs and NO<sub>x</sub>.

Firstly, a brief introduction is given on the significant automotive pollutants VOCs and  $\text{NO}_x$ , including their nature and effects on the human body. Then, the mechanism of photocatalytic oxidation technology and research advances in photocatalytic materials for removing automobile exhausts are summarized. Finally, the application (including photocatalysts combined with pavement surfaces, making photocatalysts into architectural coatings and photoreactors) of photocatalytic oxidation technology in removing the automotive exhaust is presented. We hope this review will inform the development of efficient vehicle exhaust treatment technologies.

## 2. The Main Component in Vehicle Exhaust

### 2.1. Volatile Organic Compounds (VOCs)

In recent years, a large amount of VOCs have been released into the atmosphere with industrial development [20]. Due to their highly volatile nature, VOCs can quickly enter the atmosphere and the ocean, causing extreme environmental pollution. In addition, they can also cause harm to humans through respiration [21,22]. Studies have shown that benzene is neurotoxic (causing symptoms such as neurasthenia, headaches, dizziness, and lower limb fatigue) and genotoxic (damaging DNA), putting human health at risk. Prolonged exposure can lead to anemia in humans [23,24]. Expect direct effects on human health, and many benzenes can cause photochemical smog in cities and create secondary pollution [25,26].

### 2.2. Nitrogen Oxides and Sulfur Oxides

While driving a car, the combustible mixture (fuel + air), under the influence of high temperatures and pressures and electric sparks, and other factors, causes a chemical reaction to occur that produces  $\text{NO}_x$  [27,28]. Data published by the Ministry of Ecology and Environment (MOE) in its Annual Report on Environmental Management of Mobile Sources in China (2020) shows that automobiles are the main contributor to total pollutant emissions, emitting more than 90% of  $\text{NO}_x$ . Under high-temperature combustion conditions,  $\text{NO}_x$  is mainly dominated by NO, which can account for about 95%. However, NO is very easy to react with  $\text{O}_2$  to produce other  $\text{NO}_x$  such as  $\text{NO}_2$ .  $\text{NO}_x$  all have different degrees of toxicity, which seriously pollute the air and environment and damage human health [29–31].

Petroleum usually contains elemental sulfur, so sulfur dioxide is produced when burned. When sulfur dioxide is dissolved in water, sulfite is formed. If the sulfite is further oxidized in the presence of PM 2.5, the main component of acid rain, sulfuric acid, is rapidly formed.

Atmospheric  $\text{NO}_x$  also can cause acid rain [32,33]. The acid rain with low pH severely harms animals and plants [34]. More seriously, acid rain can accelerate buildings and cultural relics' corrosion and weathering process, causing damage to buildings and bridges [35,36]. Secondly,  $\text{NO}_x$  can form photochemical smog with a special odor.  $\text{NO}_x$  in automobile exhaust can react with hydrocarbons in sunlight to form photochemical smog [37]. The composition of photochemical smog is complex and includes secondary pollutants such as ozone, aldehydes, ketones, and acids. They harm humans and animals, mainly through eye irritation and by causing respiratory disorders [38,39]. Finally,  $\text{NO}_x$  and  $\text{SO}_x$  is harmful to humans. When humans breathe,  $\text{NO}_x$  and  $\text{SO}_x$  can travel through the respiratory tract into the body and cause lung and respiratory disease. For children,  $\text{NO}_x$  may cause damage to lung development, among other things [40].

## 3. Photocatalytic Mechanisms

Among advanced catalytic oxidation technologies, photocatalysis is widely known as an emerging technology. Compared with traditional catalytic oxidation technologies, photocatalysis exhibits many economic advantages. Based on energy band theory, photocatalytic oxidation technology can be divided into the following steps: when the surface of the semiconductor material is irradiated by light, if the energy of a single photon in the incident light is greater than or equal to the bandgap energy of the semiconductor, in other words, the energy difference between the top of the valence band (VB) and the bottom of the

conduction band (CB), the electrons ( $e^-$ ) in VB have the opportunity to absorb the energy of the photon and transition to CB. The  $e^-$  that migrates to CB also leaves a positively charged hole ( $h^+$ ) on VB simultaneously, and the pair of  $e^-$  and  $h^+$  with different charges will organically initiate a series of redox reactions. For vehicle exhaust gas treatment, these reactions are reflected in reducing  $NO_x$  and the oxidative decomposition of various VOCs, as shown in Figure 1. The basic mechanism of  $TiO_2$ 's photocatalytic degradation of VOCs is as Equations (1)–(8) [41–43]:

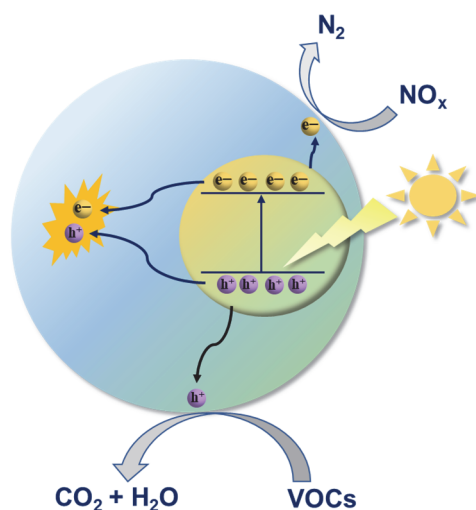
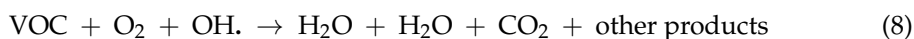
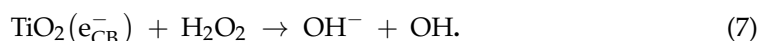
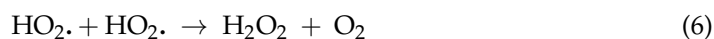
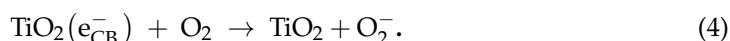
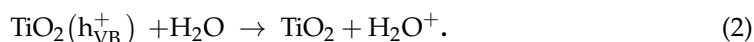
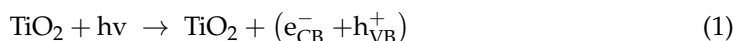


**Figure 1.** Schematic diagram of the mechanism of vehicle exhaust elimination by photocatalysis.

In the photocatalytic process, the main obstacles include two aspects: the excessively wide bandgap of the photocatalyst leads to a high energy demand for incident light and low utilization efficiency of sunlight; the other is the exciting  $e^-$  inefficiency due to recombination with  $h^+$  on VB. Since 1972, titanium dioxide ( $TiO_2$ ) has been used in water splitting for hydrogen production under ultraviolet light irradiation [44]. It has received the most research and attention as the most typical photocatalyst. Although  $TiO_2$  has exhibited good photocatalytic performance and has been widely used in commercial applications (P25  $TiO_2$  photocatalyst), only UV light can produce a photoresponse to its wide band gap ( $E_g \approx 3.2$  eV). The need for better photocatalysts has promoted the improvement work on  $TiO_2$  and stimulated researchers to explore semiconductor photocatalysts with suitable band gaps, such as Bi-based catalysts [45,46] and MOFs materials. So far, photocatalysis has shown good potential in vehicle exhaust treatment research.

## 4. Advances in Research on Photocatalytic Materials

### 4.1. $TiO_2$ -Based Materials

Among the various photocatalysts,  $TiO_2$  is one of the most responsive catalysts to UV light. Due to its low price and high activity, it is also the most widely used photocatalyst.

The limitation is that conventional TiO<sub>2</sub> only absorbs UV light, which will result in a low activity of TiO<sub>2</sub> under solar irradiance. Table 1 provides examples of reported TiO<sub>2</sub>-based photocatalysts for VOC treatment.

**Table 1.** TiO<sub>2</sub>-based materials for VOC treatment.

Photocatalyst	Preparation	Pollutants	Degradation Efficiency	Stability	Advantages	Disadvantages	Ref.
TiO <sub>2</sub>	Sol-gel	Acetone, toluene, <i>p</i> -xylene	77–62%	/	The glass spring is used as the carrier of the TiO <sub>2</sub> film, which has a good transparency and long light diffusion distance.	Small specific surface area, slow degradation rate	[47]
TiO <sub>2</sub>	Sol-gel	Toluene	52%	/	Large specific surface area	More than 420 °C are renewable	[48]
C-TiO <sub>2</sub>	Hydrothermal	Toluene	>60%	/	Green preparation method, high visible light responsiveness	High preparation temperature	[49]
Pt-rGO-TiO <sub>2</sub>	solvothermal	Benzene	95%	50 h	High activity	High cost	[50]
Ln <sup>3+</sup> -TiO <sub>2</sub>	Sol-gel	Benzene, toluene, ethylbenzene, <i>o</i> -xylene	22–79%	/	Large specific surface area, high adsorption capacity	Low performance at high humidity	[51]
Fe-TiO <sub>2</sub>	Sol-gel	<i>p</i> -Xylene	22%	/	Band gap could be reduced from 3.2 eV to 2.67 eV	Cumbersome preparation method	[52]
CNT-TiO <sub>2</sub>	Hydrothermal	Styrene	50%	/	Simple preparation method, such composite photocatalysts possess similar synergetic effects in both gaseous and aqueous phase photocatalysis.	Performance in visible light not shown	[53]

To that end, using nanomaterials as support materials for TiO<sub>2</sub>-based materials is one of the most promising solutions [54]. Carbon-based materials are the most frequently used, including carbon nanotubes, graphite nitride, graphene, and carbon fibers [55]. The advantage of carbon-based materials is that they have a large electron storage capacity, which improves the charge separation efficiency and active surface area of TiO<sub>2</sub>. In recent years, 3D graphene has been favored by researchers due to its mesoporous structure, which makes its application as a photocatalyst increasingly widespread. Nawaz et al. [56] synthesized three-dimensional reduced graphene oxide/TiO<sub>2</sub> aerogels (RGOT) by a simple one-step hydrothermal treatment. Compared with bare TiO<sub>2</sub>, RGOT exhibited a higher adsorption capacity and almost twice the ability to photodegrade carbamazepine. Similarly, Zhang et al. [57] conveniently assembled graphitic carbon nitride titanium dioxide-graphene aerogel composites using hydrothermal and freeze-drying methods. This composite exhibited considerable Rhodamine B (RhB) degradation due to its distinctive three-dimensional stratified multi-porous structure and the synergistic effect between components.

Furthermore, doping TiO<sub>2</sub> with metals and non-metals is another approach. The doping can diminish the band gap of TiO<sub>2</sub> energy, allowing TiO<sub>2</sub> to respond photoresponsively in visible light. Meanwhile, doping can enhance electron trapping and interfacial charge transfers, accelerating the separation of photogenerated electrons and holes.

Wang et al. [58] realized the degradation of vehicle exhaust gas in visible light by doping V with  $\text{TiO}_2$ . Afterward, Wang et al. [59] prepared N-doped  $\text{La}_2\text{Ti}_2\text{O}_7$  by a hydrothermal method in the presence of triethanolamine (TEA). This photocatalytic material had a broader light absorption range and photocatalytic efficiency than  $\text{TiO}_2$ , exhibited good stability in cycling experiments (as shown in Figure 2), and could become a  $\text{TiO}_2$  replacement material. Moreover, the Ag and V co-doped  $\text{TiO}_2$  photocatalytic degradation of VOCs was better than that of single-dopant  $\text{TiO}_2$  [60]. As shown in Figure 3, both the doped V and Ag enhanced the internal electron transfer in the  $\text{TiO}_2$  lattice. In addition, the doped Ag enhanced the external electron transfer between Ag particles,  $\text{Ag}_2\text{O}$ , and  $\text{TiO}_2$ . Meanwhile, the surface area of the photocatalysts co-doped with V and Ag was more extensive than that of the un-doped and single-doped photocatalysts. The co-doping of V and Ag played a synergistic role in enhancing the photocatalytic activity of  $\text{TiO}_2$ .

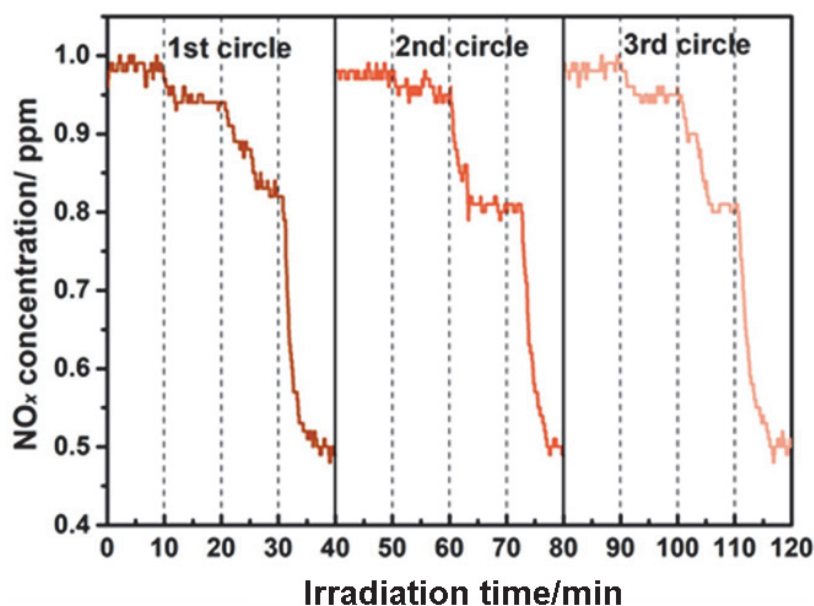


**Figure 2.** Recycling tests of photocatalytic NO degradation by N-LTO\_NC (650). (Reprinted with permission from Ref. [59]. Copyright 2021, copyright Elsevier).

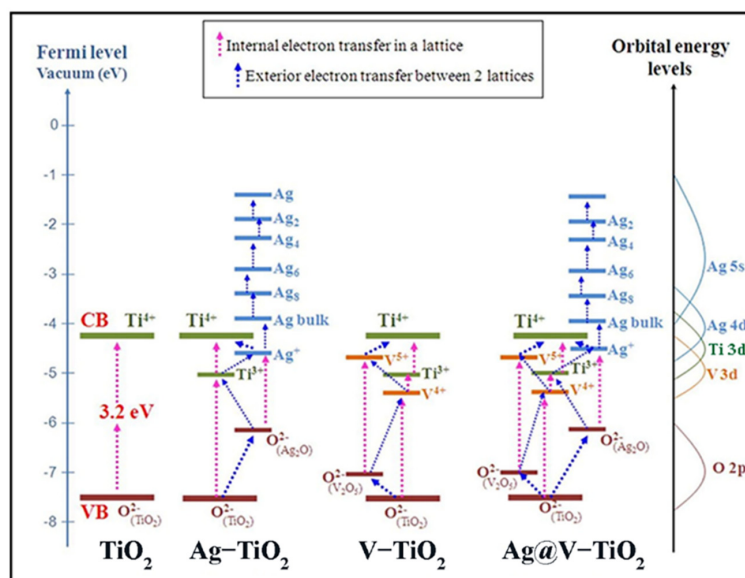


**Figure 3.** Mechanism of electron transfer in  $\text{TiO}_2$  and doped  $\text{TiO}_2$  materials. (Reprinted with permission from Ref. [60]. Copyright 2017, copyright Elsevier).

However, doping metals or non-metals in  $\text{TiO}_2$  is not perfect. The doping of non-native elements could introduce impurities of other elements and lead to a decrease in crystallinity. In addition, the doped elements could act as recombination centers, accelerating the recombination of photogenerated electrons and holes. At last, even with good doping properties, some precious metals such as rhodium, gold, and platinum were expensive and difficult to be industrially promoted. The self-doping of  $\text{Ti}^{3+}$  could avoid these disadvantages. Therefore,  $\text{Ti}^{3+}$  self-doping is one of the most promising ways to improve the photocatalytic activity of pure  $\text{TiO}_2$ .

#### 4.2. Bi-Based Materials

$\text{BiVO}_4$ ,  $\text{Bi}_2\text{WO}_6$ , and  $\text{Bi}_2\text{MoO}_6$ , as striking semiconductor materials, have become a hot spot for photocatalytic research due to their stable crystal structure, high light quantum, outstanding electron transport efficiency, and high energy utilization capability. Nevertheless, the conventional  $\text{BiVO}_4$ ,  $\text{Bi}_2\text{WO}_6$ , and  $\text{Bi}_2\text{MoO}_6$  have a low specific surface area and poor quantum utilization [61]. Recently, tremendous research efforts have been devoted to improving its photocatalytic performance.

Carbon quantum dots (CQDs) had an excellent ability to extend the visible absorption region and suppress photogenerated electron and hole complexes. Thus, Qian et al. [62] combined CQDs with  $\text{Bi}_2\text{WO}_6$  to fully utilize solar energy for photocatalytic VOC removal. Furthermore, Meng and Zhang [63] prepared Pd-rGO- $\text{Bi}_2\text{MoO}_6$  ternary photocatalyst composites using a solvothermal-photoreduction method, as the prepared composites exhibited outstanding visible light photocatalytic activity, especially for applications in the degradation of organic pollutants. That advantage appeared to be explained by three factors. Firstly, the reduced graphene oxide layer could be used as an electron acceptor so that light-generated electrons could be quickly transferred to its surface instead of binding to positively charged holes. In addition, the blackbody properties of graphite-like materials contributed to improving visible light photon capture. Finally, due to the surface plasmon resonance effect, the Pd nanoparticles located on the surface could be excited by visible light photons, which further improved the efficiency of the utilization of visible light radiation.

The heterojunctions can limit the recombination of photogenerated carriers and enhance the light trapping of photocatalysts. Various  $\text{Bi}_x\text{MO}_y$ -based heterojunction structures have successfully synthesized and shown excellent photocatalytic performance. In a heterojunction, the energies of the two crystals reach equilibrium by unifying the Fermi energy levels while generating an internal electric field [61]. Meng et al. [64] successfully prepared an interspersed QDs  $\text{MoS}_2$ - $\text{Bi}_2\text{WO}_6$  heterostructure using a simple bath sonication method. The p-n heterostructure between  $\text{MoS}_2$  and  $\text{Bi}_2\text{WO}_6$  resulted in enhanced photocatalytic performance and a more comprehensive photoresponse range of  $\text{MoS}_2$ - $\text{Bi}_2\text{WO}_6$  compared with bare  $\text{Bi}_2\text{WO}_6$  and  $\text{MoS}_2$ . Afterward, Zhou et al. [65] synthesized silver-modified  $\text{WO}_3/\text{Bi}_2\text{WO}_6$  heterojunction with a direct Z-structure energy band structure. Compared with the pristine  $\text{Bi}_2\text{WO}_6$  and  $\text{WO}_3/\text{Bi}_2\text{WO}_6$ ,  $\text{Ag}/\text{WO}_3/\text{Bi}_2\text{WO}_6$  exhibited better photocatalytic activity for removing gaseous chlorobenzene under simulated sunlight irradiation. As shown in Figure 4, the conversion efficiencies of the pristine  $\text{Bi}_2\text{WO}_6$  and  $\text{WO}_3/\text{Bi}_2\text{WO}_6$  were 29% and 45%, respectively. In the Ag-decorated  $\text{WO}_3/\text{Bi}_2\text{WO}_6$  hybrid, the doping of different mass fractions of Ag significantly affected its performance. The degradation efficiency of 2%  $\text{Ag}/\text{WO}_3/\text{Bi}_2\text{WO}_6$  was higher than that of 0.5%  $\text{Ag}/\text{WO}_3/\text{Bi}_2\text{WO}_6$ . The 2%  $\text{Ag}/\text{WO}_3/\text{Bi}_2\text{WO}_6$  hybrid showed the highest photocatalytic degradation performance in the prepared samples, 1.8 and 2.8 times higher than the  $\text{WO}_3/\text{Bi}_2\text{WO}_6$  heterojunction and pristine  $\text{Bi}_2\text{WO}_6$ , respectively. The improved photocatalytic degradation performance is mainly due to the three-component heterojunction with a Z-shaped  $\text{Ag}/\text{WO}_3/\text{Bi}_2\text{WO}_6$  and the surface plasmon resonance effect of Ag nanoparticles, which increases the absorption of visible light and reduces the recombination rate of photogenerated carriers.

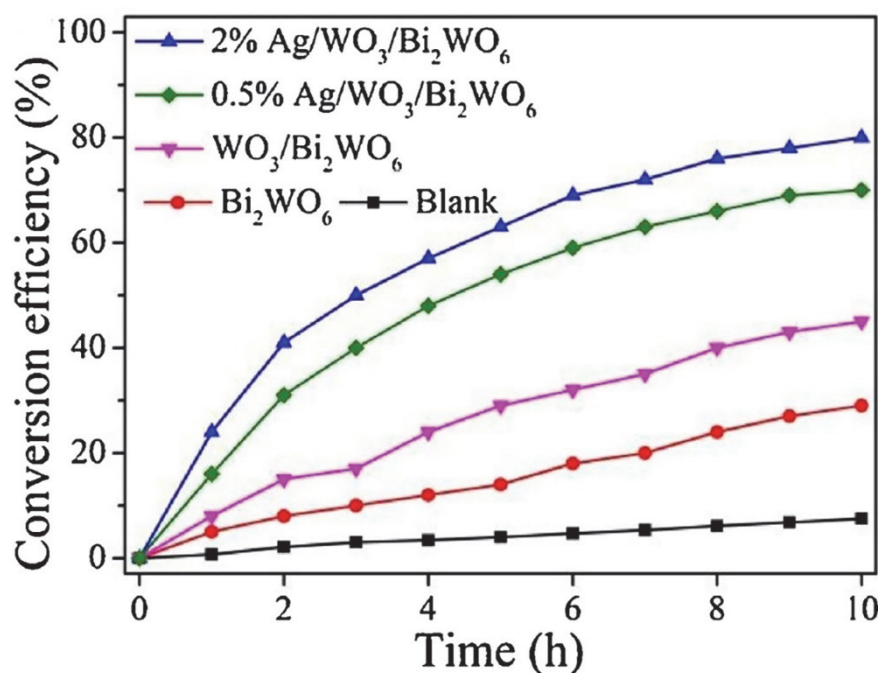


**Figure 4.** Comparison of the photocatalytic activity of the as-prepared samples for the photocatalytic degradation of chlorobenzene under simulated sunlight irradiation. (Reprinted with permission from Ref. [65]. Copyright 2019, copyright Elsevier).

Bi-based materials with suitable band gaps have been extensively researched in photocatalysis. There are still many opportunities and challenges for Bi-based photocatalysts. For example, the increase in the light absorption range leads to increased carrier recombination. In addition, the industrial applications of Bi-based photocatalysts are hindered by the instability of catalysts, the difficulty of recycling, and the secondary hazards of nanomaterials. For this reason, future work can focus on these two aspects: (i) combining doped/defective structures and heterojunction engineering to further improve photocatalyst performance; (ii) improving the understanding of recycling and reuse of Bi-based photocatalysts and practical applications.

#### 4.3. MOFs Materials

In recent years, MOFs, a novel category of porous coordination polymers, have attracted much attention because of their distinctive porous structure, large specific surface area, good thermal stability, and excellent catalytic activity [66,67].

Although MOFs with distinct advantages are good candidates for novel multiphase photocatalysts, some barriers limit their practical application in environmental remediation [68]. The wide band gap of most MOFs can only capture UV light, which means that 95% of the solar light cannot be utilized. Moreover, pure MOFs' high photogenerated electron-hole pair recombination rate leads to their low photocatalytic activity [69]. Improving the photocatalytic activity of pure MOFs by modifying them is a promising strategy. Therefore, many researchers have invested much research in modifying MOFs. Liu et al. [70] used the UiO-66-NH<sub>2</sub>@MIL-101 (Fe) heterostructure as a catalyst for photocatalytic styrene oxidation, and the strong performance of the catalyst was attributed to the dendritic structure and having proper bandgap energy. Furthermore, Zhang et al. [71] synthesized NH<sub>2</sub>-MIL-101 (Fe) hexagonal microspheres by a solvothermal method and applied them to remove gaseous toluene degradation under visible light irradiation with a conversion of 79.4%. The visible light absorption of MIL-101 (Fe) was made possible by introducing NH<sub>2</sub>.

Based on these works, attaining functionalized MOFs by modifying pure MOFs is considered a feasible solution to enhance the performance of photocatalysts. MOF-based

photocatalysts possess distinct advantages compared with other semiconductor-based photocatalysts. Firstly, organic and inorganic compounds in MOFs provide enhanced structural stability. Besides, MOF structures with tunable components can effectively promote the separation and transfer rate of photogenerated  $e^-$  and  $h^+$ . Moreover, the numerous light absorption sites of MOFs benefiting from the high porosity have expanded the light absorption range. However, the MOFs still have many challenges as novel photocatalysts. First, the low space–time yield still limits the large-scale treatment of natural indoor air. In addition, catalyst performance is still unsatisfactory. Common MOF-based photocatalyst systems typically have lower oxidation than conventional metal oxide photocatalysts (e.g.,  $TiO_2$ ). Such poorer mineralization can result in the accumulation of organic intermediates on the photocatalyst surface, leading to catalyst deactivation and hindering the catalytic cycle [72]. Lastly, the degradation of MOFs' organic structures upon prolonged exposure to light is a significant factor limiting MOF materials as photocatalysts [73,74].

### 5. Application of Photocatalysis to Remove Vehicle Exhaust Emissions

For removing 1% of residual exhaust gases from untreated automotive exhaust systems, this section presents advances in photocatalytic technology for treating residual automotive exhaust gases from pavement materials, architectural coatings, and photocatalytic reactors. Table 2 provides examples of the reported photocatalytic treatment of vehicle exhaust gas.

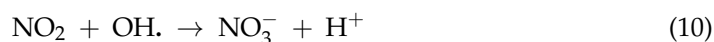
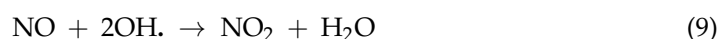
**Table 2.** Photocatalytic treatment of vehicle exhaust gas.

Pollutants	Concentration	Photocatalyst	Light Type	Efficiency	Irradiation Time	Ref.
Mixture of toluene, decane, and trichloroethylene (TCE)	1–1000 ppb	$TiO_2$	UV light	77%	40 h	[75]
Toluene, methanol, and ethyl acetate	2.7 g/m <sup>3</sup>	$TiO_2$ -RGO/LDHs	Simulated sunlight	69.9%, 91.6% and 99.9%	1 h	[62]
Acetaldehyde, formaldehyde, and trichloroethylene	1000 ppm	Decahedral anatase titania particles (DAPs)	UV light	$5.10 \mu\text{mol}\cdot\text{s}^{-1}\cdot\text{g}_{\text{cat}}^{-1}$	12 h	[76]
Chloroform and glutaraldehyde	4–40 mg/m <sup>3</sup>	$TiO_2$ /optical fiber photocatalyst	UV light	$k = 0.0463 \text{ mmol}\cdot\text{m}^{-3}\cdot\text{s}^{-1}$	2 h	[77]
Butane-2,3-dione ( $C_4H_6O_2$ ) and Heptan-2-one ( $C_7H_{14}O$ )	5–20 mg/m <sup>3</sup>	Cu-Ag/ $TiO_2$ -based optical fibers	UV light	52% and 50%	12 h	[78]
Isopropanol (IPA)	1.8–14.6 ppm	$TiO_2$	UV light	99%	1 h	[79]
<i>n</i> -hexane	1–25 ppm	Sol-gel $TiO_2$ -anatase	UV light	$k = 1.9 \times 10^{-6} \text{ mol m}^{-3} (\text{W m}^{-2})^{-0.65} \text{ g}^{-1} \text{ s}^{-1}$	/	[80]
Toluene and acetone	28 and 106 mg/m <sup>3</sup>	$TiO_2/H_2Ti_3O_7$	UV light	91.5% and 92.5%	2.5 h	[81]
$NO_x$	822 ppm	$TiO_2$	UV light	$k = 2.6\sim 5.9 \times 10^{-4} \text{ s}^{-1}$	/	[82]
$NO_x$	1–2 ppmv	$TiO_2$	UV light	10–12%	24 h	[83]
$NO_x$	40 ppbv	$TiO_2$	UV light	100%	6 h	[84]



### 5.1. Fixing the Photocatalyst to the Pavement

The pavement is the location of the highest concentration of vehicle emissions in the external environment. Therefore, treating exhaust pollution on the pavement is the obvious choice. Ma et al. [85] had added TiO<sub>2</sub> nanoparticles directly to asphalt and continuously stirred it at 170 °C to obtain samples with degradation activity against NO<sub>x</sub> and CH. Mahy et al. [86] developed a TiO<sub>2</sub>-based photocatalytic coating for degrading the significant components of vehicle exhaust, such as NO<sub>x</sub> and organic compounds. The study began with the coating deposition on pavement blocks, brushes, or exposed aggregate road concrete using dipping or spraying techniques. The performance of all samples was tested for the photocatalytic degradation of NO<sub>x</sub>. All samples, except that obtained from the sol-gel organic pathway, showed NO<sub>x</sub> degradation rates ranging from 10% to 45%. Abrasion and freeze-thaw tests on these coatings with photocatalysts showed excellent stability. TiO<sub>2</sub> is cheap, readily available, and has high photocatalytic activity, so most of the current practical applications of the photocatalytic treatment of vehicle exhaust are based on TiO<sub>2</sub>. The reduction of NO<sub>x</sub> to non-toxic and non-hazardous N<sub>2</sub> is the ideal solution. However, the following reaction processes, as Equations (9)–(11), must not be neglected.



This series of reactions produces HNO<sub>3</sub> that causes deactivation of the catalyst, especially when the air humidity is high. It seriously affects the lifetime of the catalyst.

For enhancing the photocatalytic stability and activity of TiO<sub>2</sub> on the pavement, Yu et al. [87] prepared nano-TiO<sub>2</sub> coating materials for the pavement and roadside using anatase-type nano-TiO<sub>2</sub>, activated carbon powder, silane coupling agent, and deionized water. Different mass ratios of sodium dodecylbenzene sulfonate for the curb coating were added as surfactants. The material showed the best catalytic degradation when the mass ratio of nano-TiO<sub>2</sub> to surfactant was about 1:2. Furthermore, Singh et al. [88] optimized the parameters for the degradation of SO<sub>2</sub> and NO<sub>2</sub> by asphalt pavement loaded with TiO<sub>2</sub>. The optimal concentration of TiO<sub>2</sub> slurry ranged from 25 to 125 mL m<sup>-2</sup>, the optimal range of UV-A irradiance was 1 to 5 mW cm<sup>-2</sup>, and the optimal percentage of asphalt was 4% to 6%. These parameters achieved the highest degradation rates of SO<sub>2</sub> and NO<sub>2</sub> for TiO<sub>2</sub>-loaded asphalt pavements.

In addition, to improve the wear resistance of photocatalysts on pavement, Wang et al. [89] developed a new asphalt pavement coating method in which finely ground TiO<sub>2</sub> cement mortar was laid on the pavement, and epoxy resin was applied to its surface after drying to immobilize the catalyst on the pavement. The long-term NO<sub>x</sub> removal efficiency, abrasion resistance, and skid resistance of asphalt pavement coatings applying this fixing method were tested. The study results showed that the method can achieve long-lasting NO<sub>x</sub> degradation efficiency and is feasible in practical applications.

All the above work was carried out with pure TiO<sub>2</sub> particles as catalysts. However, two primary issues had to be addressed to enhance the photocatalytic activity of TiO<sub>2</sub>. In the first place, the nano-TiO<sub>2</sub> with a bandgap of 3.2 eV could not be excited when the wavelength of light is more significant than 384 nm [90]. In addition, TiO<sub>2</sub> had a high recombination rate of photogenerated electrons and holes, reducing the number of electron holes involved in the redox reaction and suppressing catalytic activity [91]. Therefore, the modification of TiO<sub>2</sub> mentioned in Section 4 is an essential tool for improving the photocatalytic performance of TiO<sub>2</sub> in degrading vehicle exhaust and expanding the wavelength range of the optical response.

Further enhancing the photocatalytic activity, anatase-type TiO<sub>2</sub> was modified by doping with Nitrogen (N) by Zhang et al. [92] resulting in an N doped TiO<sub>2</sub> (N-TiO<sub>2</sub>). Anatase-type TiO<sub>2</sub> and N-TiO<sub>2</sub> were prepared by sol-solvothermal, and analyses through

CASTEP showed the bandgap of N-TiO<sub>2</sub> was reduced. It was shown that the photocatalytic degradation activity of N-TiO<sub>2</sub> was higher than pristine TiO<sub>2</sub>. As shown in Figure 5a, UV-Vis DRS results indicated that N doping caused a redshift in the absorption band. The prepared material was tested in the photocatalytic degradation of exhaust pavement using NO and CO as the model exhaust fumes (Figure 5b,c). The results showed that the N-TiO<sub>2</sub> is more suitable for stone mastic asphalt pavement. This research provided novel ideas for the degradation of road exhaust and new pavement materials for the degradation of vehicle exhaust.

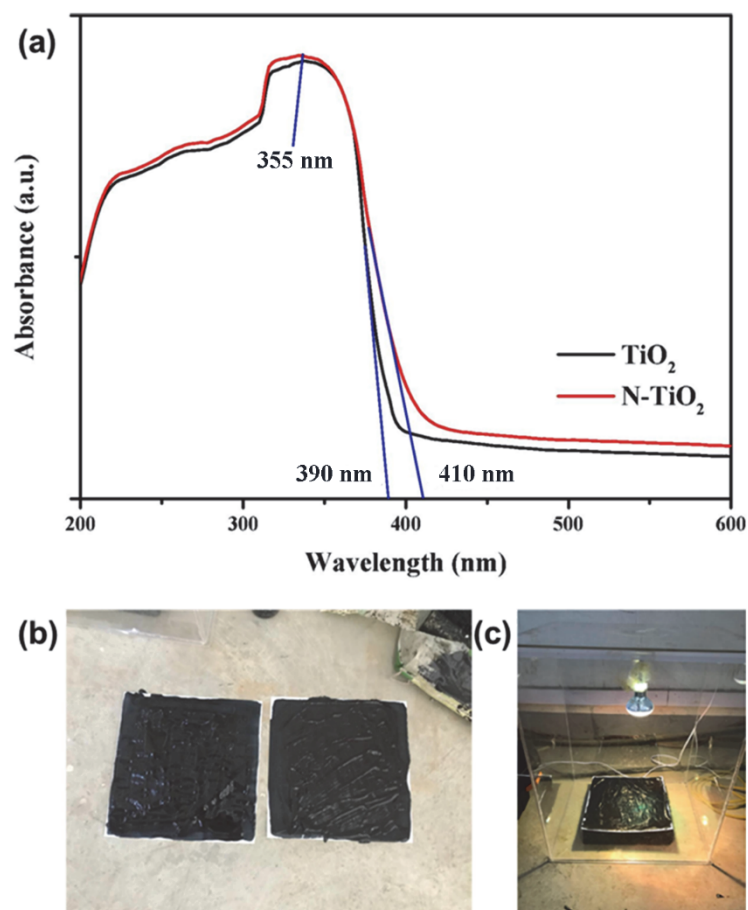


**Figure 5.** (a): UV-Vis DRS of TiO<sub>2</sub> and N-TiO<sub>2</sub>. Experimental device (b): Cardboard coated with emulsified asphalt and (c): Simulating the experimental process of solar irradiation. (Reprinted with permission from Ref. [92]. Copyright 2021, copyright Elsevier).

Hu et al. [93] used the method of loading Fe-doped TiO<sub>2</sub> onto biomass-activated carbon to expand the spectral response range of TiO<sub>2</sub> and improve the photocatalytic performance of TiO<sub>2</sub>. The non-lattice oxygen generated by substituting Fe<sup>3+</sup> for Ti<sup>4+</sup> was more attractive to the adsorbed oxygen and hydroxyl groups, and the Fe doping improved the photocatalytic activity of TiO<sub>2</sub>. In addition, the photo-responsive region of Fe-doped TiO<sub>2</sub> was red-shifted to the visible region, with a maximum wavelength of light absorption of 550 nm. In pavement test experiments, the catalyst effectively degraded both CH and NO<sub>x</sub>. The combined results of the above work led to the conclusion that TiO<sub>2</sub> was the most efficient in degrading NO<sub>x</sub> and unsatisfactory in degrading CO<sub>2</sub> and CO. This was because NO<sub>x</sub> is acidic and combines effortlessly with alkaline-hardened cement paste surfaces. At the same time, the purification process of CO<sub>2</sub> and CO is reversible and incompatible with the Langmuir-Hinshelwood (L-H) reaction model.

Most current photocatalytic degradation of road vehicle exhaust applications is based on TiO<sub>2</sub> catalysts, but the combination of catalyst and bitumen is varied. Photocatalytic

materials for asphalt pavements can be applied in two primary methods: mixing and coating. The mixing method involves adding the photocatalyst to the asphalt mixture to make the pavement material, resulting in only a minority of the catalyst being exposed to sunlight, causing a substantial waste of the catalyst. The coating method involves adding the catalyst to a solvent or preparing a sprayed coating onto the pavement. Obviously, this method saved the catalyst, but as the wheels crushed, the catalyst would fall off, and the amount of catalyst decreased, resulting in rapidly decreasing catalytic performance. In addition, the coating decreased the skid resistance of the road surface, which increased the risk of driving [94]. We have proposed a new method to fix the catalyst on the pavement, and therein the disadvantages of these two methods. After the asphalt mix was paved and initially rolled, the catalyst powder was sprayed uniformly onto the surface of the asphalt mix and then rolled several times. This method allowed the catalyst to be exposed to sunlight to maximize photocatalysis and gave the catalyst good wear resistance, with little impact on pavement performance.

### 5.2. Manufacturing Photocatalysts into Architectural Coatings

The areas around roads with heavy traffic are the most polluted by vehicle emissions. In addition to the pavements, the buildings on both sides of the road should also be considered. Photocatalysts are made into paint and applied to the facades of buildings and railings on both sides of the road, allowing them to degrade car emissions.

Brattich et al. [95] demonstrated the potential effectiveness of photocatalysis in natural climatic conditions by testing the photocatalytic activity of TiO<sub>2</sub> coatings for NO<sub>x</sub> in a real-world street canyon and showed a range of 14–21% for the photocatalytic reduction of NO<sub>x</sub>. In addition, Qian et al. [96] prepared a carbon foam material from polyurethane foam and phenolic resin, followed by wet oxidation to process the carbon foam into hydrophilic carbon foam with many carboxyl groups. The mesoporous TiO<sub>2</sub> films were deposited on the carbon foam, which acted as a carrier for the TiO<sub>2</sub> films and an adsorbent for harmful gases such as VOCs. Researchers have made numerous efforts to enhance the photocatalytic activity of TiO<sub>2</sub> coatings. Lorencik et al. [97] modified the effect of a carbon-doped TiO<sub>2</sub> suspension by adding nanostructured silica to develop a photocatalytic coating to eliminate indoor gas pollutants. NO<sub>x</sub> removal experiments showed that the addition of nanostructured silica improved the photocatalytic efficiency of the coating. Sansotera et al. [98] proposed a method for immobilizing TiO<sub>2</sub> nanoparticles: TiO<sub>2</sub>-containing perfluorosulfonic acid polymers were covered with a layer of perfluorinated amorphous polymers and evaluated for their applicability in the gas-phase photocatalytic degradation of six different VOCs (pentane, methanol, isopropanol, toluene, methylene chloride, and pyridine). Moreover, it was also confirmed that atmospheric conditions (namely, humidity) and the nature of the contaminant (polarity, primary nature) strongly influenced the photodegradation kinetics of the TiO<sub>2</sub> coating.

The stability of the photocatalyst coating is also a critical factor in determining whether it could be widely used. Consequently, Rosset et al. [99] added TiO<sub>2</sub> nanoparticles to the coating to test the possibility of its practical application. The results showed that the photocatalytic coating containing nano-titania could maintain high stability for 1000 h. It was worth mentioning that Morin et al. [100] found that the TiO<sub>2</sub> coating may decompose the binder, which causes additional VOCs while causing the catalyst to fall off and be loose. Therefore, the connection method of TiO<sub>2</sub> to the carrier material and the potential impact on the environment is still worthy of further design and consideration in practical applications.

### 5.3. Photocatalytic Reactors

Fixing the photocatalyst to the pavement and manufacturing photocatalysts into architectural coatings, already described in Sections 5.1 and 5.2, are promising technologies for automotive exhaust remediation. However, measuring the air cleaning durability of these methods is incredibly time-consuming. Designing a reasonable photocatalytic reactor is a possible way to evaluate the photocatalysts' surface activity rapidly and reliably.

Besides, a highly efficient photocatalytic reactor can be used as a stand-alone vehicle exhaust treatment system. The installation of highly efficient photocatalytic reactors at the roadside can effectively reduce the concentration of vehicle exhaust. Consequently, advances in the development and application of photocatalytic reactors in recent years, including packed-bed reactors, microreactors, and other advantageous reactors, are reviewed.

### 5.3.1. Packed-Bed Reactors

The packed-bed reactor is filled with a tiny solid catalyst of a specific particle size to a certain height in a transparent reaction pipe. The gas to be treated enters the reactor through a blower and passes through the catalyst-filled bed, and a catalytic reaction occurs in the filled bed. Lamps surround the reaction pipe to provide the light source for the photocatalytic reaction. The inlet and outlet sections of the reaction tube are filled with porous materials (e.g., foam, asbestos, and textiles) that do not contain a catalyst to provide a stable airflow and prevent the catalyst from escaping from the tube with the airflow.

Fernandez-Catala et al. [101] used a sample dispersion (P25) in ethanol to obtain a packed bed structure. The photocatalyst (P25) was immobilized in a capillary tube, and a surfactant (F-127) was added to produce fine pore channels in the microreactor, as shown in Figure 6a,b. The microreactor's photocatalytic activity per molar photocatalyst (P25) was significantly increased in the experiment with the of removal propene; the experimental setup is shown in Figure 6c. Furthermore, the microcolumns with a specific porosity in the P25 particles presented the best photocatalytic performance. The pressure drop was comparable to a conventional reactor using a thin P25 bed. It is crucial to determine the appropriate gas flow rate for a packed bed reactor. A low gas flow rate would lead to low degradation efficiency; an excessive gas flow rate would lead to the catalyst escaping and even channel flow formation. Therefore, it places a higher demand on the gas flow stability, which is a disadvantage of a packed bed reactor.

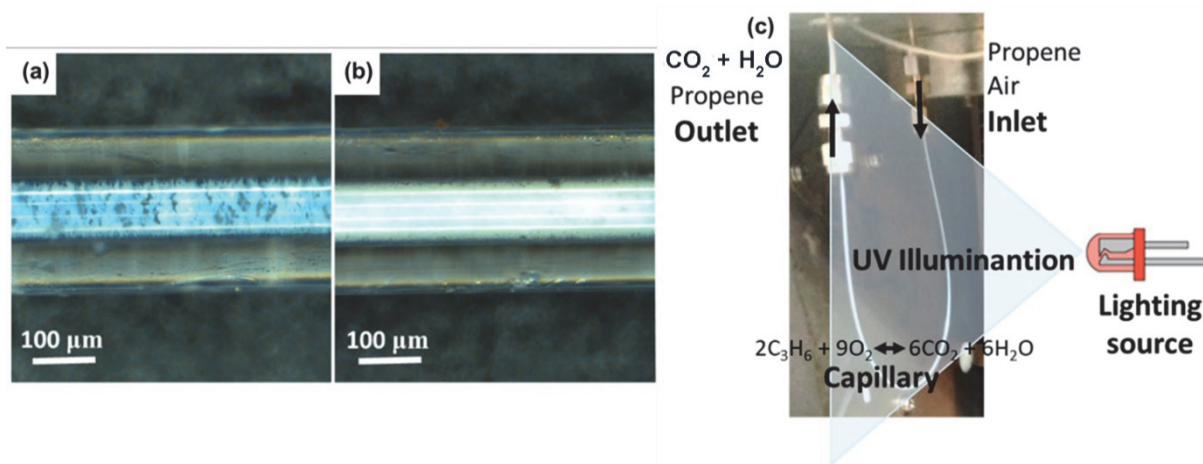


**Figure 6.** Microscope images of the different filled capillaries prepared in this study: (a) Cap. P25/F-127; (b) Cap. P25. (c) Illustration of the experimental setup used for the photocatalytic oxidation of VOCs. (Adapted from Ref. [101]).

To address the disadvantage, appropriately increasing the particle size of the packing material is an effective method. Damyar et al. [102] measured the efficiency of a packed-bed plasma reactor in the  $\text{SO}_2$  removal process, eventually optimizing it using a central composite design approach. The results showed that the packed-bed plasma reactor offers significant energy savings and high  $\text{SO}_2$  removal efficiency, which was at least twice as high as the unpacked plasma reactor. However, the performance of the in-plasma catalytic reactor decreased with time. Filled-bed plasma reactors were no longer affected by the bed's destruction by high gas flow rates.

Despite its many disadvantages, the packed-bed reactor still has the advantages of fast mass transfer and a simple structure for treating gases. The combination of other reactors with the packed-bed reactor can be considered in future research, which may achieve unexpected results.

### 5.3.2. Microreactors

In recent years, microreactors have received particular attention due to the unique properties of microspecies. In contrast to other reactors, microreactors can address internal mass transfer and illumination issues. Microfluidic devices with favorable characteristics for improved photon transport are potentially suitable for photocatalytic reactions. Furthermore, it also had the characteristics of a short molecular diffusion distance, fast heat dissipation, and high efficiency.

Poulakis and Philippopoulos [103] tested five photocatalysts (TiO<sub>2</sub> isopropoxide, TiO<sub>2</sub> P25, and TiO<sub>2</sub>-P25 with 1% Pt, Fe, or Ce) in a miniature annular reactor to remove vehicle exhaust gases (the experimental apparatus in Figure 7). Pt-TiO<sub>2</sub> P25 exhibited the most significant activity in removing NO and hydrocarbons and promoting hydrocarbon oxidation under feed-depleted conditions and NO reduction under feed-rich conditions, with behavior similar to that of commercial triple-acting catalysts. The absence of NO<sub>2</sub> production was observed in the NO decomposition/oxidation reaction in water and no deactivation of the catalyst, which suggested a favorable selectivity of Pt-TiO<sub>2</sub> P25 for N<sub>2</sub> production. Ola and Maroto-Valer [104] designed a monolithic microreactor for photocatalytic CO<sub>2</sub> reduction. The interior of the reactor was a 100-hole/square-inch cordierite honeycomb monolith with a diameter of 40 mm and a length of 50 mm. A total of 177 non-coated side-light-emitting optical fibers crossed the coated monolith, enabling uniform light distribution in the internal channels. The photocatalytic activity of the monolithic structure coated with pure TiO<sub>2</sub>, Cr, V, or Co-TiO<sub>2</sub> was measured under visible light irradiation. The reactor with a simple structure and a large surface area has a broad future in the photocatalytic treatment of automotive exhaust gases.

The trend has been towards the miniaturization of reactors, which poses higher technological requirements for reactor fabrication. Especially for micro photocatalytic reactors, the fixation of the catalyst poses a challenge, and the emerging 3D printing technology may be a solution.

### 5.3.3. Other Reactors

In addition to packed-bed reactors and microreactors, several other photoreactors used to treat hazardous gases were reviewed. These reactors have particular structures and advantages.

As shown in Figure 8a, Pellegrino et al. [105] developed a portable, continuously stirred continuous flow photoreactor system that can measure photocatalytic activity quickly and reliably. The effective contact surface of the reactor with the measured surface was a circle with a diameter of four centimeters. A gasket system at the contact port ensured a good seal, enabling in situ measurements. The reactor offers several advantages in terms of time and cost, making it easy to control the durability of the deployed photocatalytic material on rough surfaces. Héquet et al. [106] designed a closed-loop photocatalytic reactor with a volume of 420 L. The reactor consists of a flat geometric photocatalytic filter, four UVA lamps, a fan, and an air purification chamber. Bellè et al. [107] produced TiO<sub>2</sub> built-in nanotubes by anodic oxidation, applied them to a novel annular plug flow reactor, and tested the photocatalytic degradation of toluene. The photocatalytic system exhibited a photodegradation efficiency of up to 90% when the concentration of toluene entering the reactor was 10 ppm. Therefore, the reactor had the potential for application in lightly polluted environments. However, the initial degradation rates ranged from 60% to 70%. Subsequently, the degradation rate gradually decreased due to the deactivation of the photocatalyst, which was attributed to the accumulation of refractory by-products at the adsorption site that occupied the catalyst's active site. Therefore, the reactor was more suitable for degrading

low concentrations of toluene. Gao et al. [108] prepared PdAg/AgBr/TiO<sub>2</sub> photocatalytic layered nanostructures using a hydrothermal method and used this bimetal-supported composite catalyst for the photocatalytic degradation of propylene. This nano-level structure effectively improved the charge separation ability in AgBr and TiO<sub>2</sub> and improved VOC's degradation efficiency. A continuous photocatalytic reactor with good degradation efficiency for VOCs was also designed, as shown in Figure 8b.

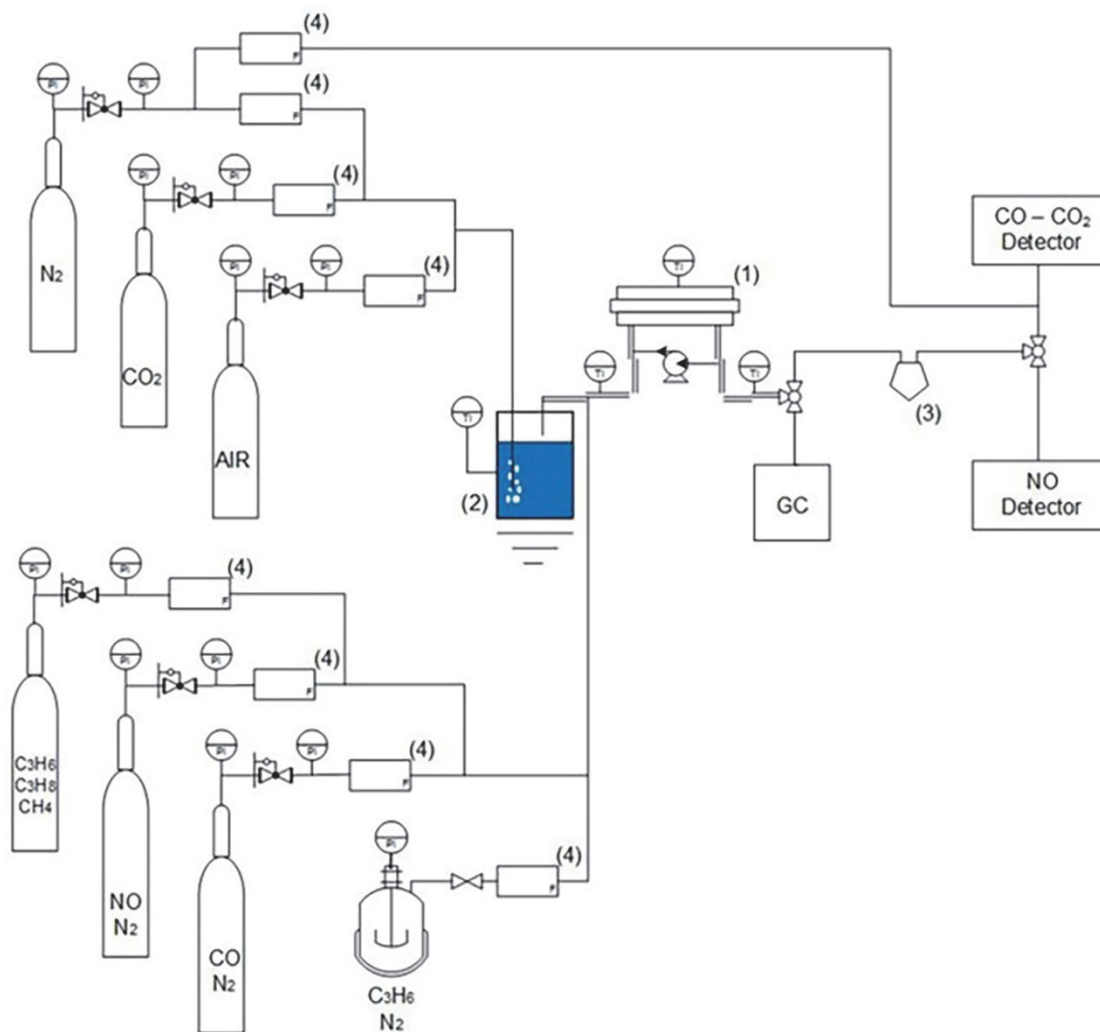


**Figure 7.** The experimental apparatus: (1) reactor, (2) thermostatic water bubbler, (3) water trap, and (4) mass flow controllers. (Reprinted with permission from Ref. [103]. Copyright 2017, copyright Elsevier).

The objectives of developing photocatalytic reactors were to provide more active sites for catalytic reactions and improve photocatalytic efficiency. On the other hand, developing a rational reactor could accelerate the experimentation of novel photocatalytic materials and promote photocatalysis's application to eliminate vehicle exhausts. We could consider the implementation of efficient aqueous-phase photocatalytic reactors into the gas phase to accelerate the development of gas-phase photocatalytic reactors, such as the slant-plate photoreactor designed by Zhao et al. [109].

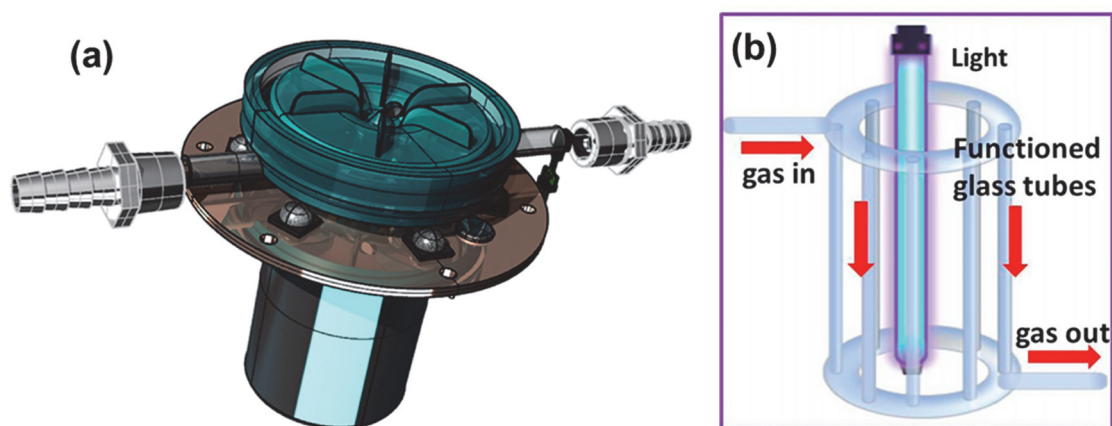


**Figure 8.** (a) 3D rendering of the reaction chamber with the fan and the LED source. (Reprinted/adapted with permission from Ref. [105]. Copyright 2020, copyright Elsevier) (b) Design of the continuous photocatalytic device for gas-phase degradation. (Reprinted with permission from Ref. [108]. Copyright 2018, copyright Elsevier).

## 6. Conclusions and Perspectives

In summary, there have been many studies on the photocatalytic treatment of VOCs and  $\text{NO}_x$  in vehicle exhaust, ranging from the innovation of photocatalytic materials to reactor design and coating inspection. As a developing research area, more contributions are required to understand this process further. The following recommendations for future works should be considered:

- i. The implementation of photocatalytic oxidation technology in practice has restricted the low efficiency of photocatalysis. It is feasible to use photocatalysis in synergy with thermal catalysis to accelerate the degradation rate of vehicle exhausts. Photothermal catalysis as a novel strategy, especially in the hot summer months, can reduce vehicle emissions more effectively.
- ii. The release of additional VOCs caused by photocatalysts is a potential factor that plagues the application. Therefore, while developing new photocatalysts with better performance, it may be a more feasible strategy to consider coupling photocatalytic technology with other high-efficiency technologies.
- iii. According to previous studies, most experiments have been carried out under high concentrations of car exhaust, which is far from the actual situation on the road. Therefore, it is essential to extend the research to the natural roadside conditions.
- iv. Various factors affect the photocatalytic degradation rate of vehicle exhaust. Therefore, the effects of relative humidity, air velocity, catalyst carrier material, and fixation method should be considered in the practical application of photocatalysis.
- v. Although photoreactors can enhance photocatalytic efficiency, the application has several limitations. Therefore, combining different photoreactors may be the future direction of photoreactors. In this way, these photoreactors' advantages are fully utilized and provide significant synergistic effects.

We hope that the present review will provide critical research advances in photocatalysis for removing vehicle exhaust, and we expect more photocatalytic technologies to be used to remove vehicle exhaust shortly.

**Funding:** The authors acknowledge the financial supports from China Postdoctoral Science Foundation (Grant No.: 2020M682241), the Fundamental Research Funds for the Central Universities (Grant No.: 202013050), Shandong Provincial Natural Science Foundation (Grant No.: ZR2021QB056).

**Conflicts of Interest:** The authors declare that they have no known competing financial interests or personal relationships that could have appeared to influence the work reported in this paper.

## References

1. Sinay, J.; Puskar, M.; Kopas, M. Reduction of the NO<sub>x</sub> emissions in vehicle diesel engine in order to fulfill future rules concerning emissions released into air. *Sci. Total Environ.* **2018**, *624*, 1421–1428. [[CrossRef](#)] [[PubMed](#)]
2. Winkler, S.L.; Anderson, J.E.; Garza, L.; Ruona, W.C.; Vogt, R.; Wallington, T.J. Vehicle criteria pollutant (PM, NO<sub>x</sub>, CO, HCs) emissions: How low should we go? *Npj Clim. Atmos. Sci.* **2018**, *1*, 26. [[CrossRef](#)]
3. Suarez-Bertoa, R.; Valverde, V.; Clairotte, M.; Pavlovic, J.; Giechaskiel, B.; Franco, V.; Kregar, Z.; Astorga, C. On-road emissions of passenger cars beyond the boundary conditions of the real-driving emissions test. *Environ. Res.* **2019**, *176*, 108572. [[CrossRef](#)]
4. Moreno, T.; Pacitto, A.; Fernandez, A.; Amato, F.; Marco, E.; Grimalt, J.O.; Buonanno, G.; Querol, X. Vehicle interior air quality conditions when travelling by taxi. *Environ. Res.* **2019**, *172*, 529–542. [[CrossRef](#)] [[PubMed](#)]
5. Lambert, C.K. Current state of the art and future needs for automotive exhaust catalysis. *Nat. Catal.* **2019**, *2*, 554–557. [[CrossRef](#)]
6. Gandhi, H.S.; Graham, G.W.; McCabe, R.W. Automotive exhaust catalysis. *J. Catal.* **2003**, *216*, 433–442. [[CrossRef](#)]
7. Shelef, M.; Graham, G.W. Why Rhodium in Automotive Three-Way Catalysts? *Catal. Rev.* **2006**, *36*, 433–457. [[CrossRef](#)]
8. Farrauto, R.J.; Deeba, M.; Alerasool, S. Gasoline automobile catalysis and its historical journey to cleaner air. *Nat. Catal.* **2019**, *2*, 603–613. [[CrossRef](#)]
9. Batterman, S.; Jia, C.; Hatzivasilis, G. Migration of volatile organic compounds from attached garages to residences: A major exposure source. *Environ. Res.* **2007**, *104*, 224–240. [[CrossRef](#)]
10. Li, Y.W.; Ma, W.L. Photocatalytic oxidation technology for indoor air pollutants elimination: A review. *Chemosphere* **2021**, *280*, 130667. [[CrossRef](#)]
11. Michael, S.G.; Michael-Kordatou, I.; Beretsou, V.G.; Jäger, T.; Michael, C.; Schwartz, T.; Fatta-Kassinos, D. Solar photo-Fenton oxidation followed by adsorption on activated carbon for the minimisation of antibiotic resistance determinants and toxicity present in urban wastewater. *Appl. Catal. B Environ.* **2019**, *244*, 871–880. [[CrossRef](#)]
12. Sanito, R.C.; You, S.J.; Wang, Y.F. Degradation of contaminants in plasma technology: An overview. *J. Hazard. Mater.* **2022**, *424*, 127390. [[CrossRef](#)] [[PubMed](#)]
13. Karatum, O.; Deshusses, M.A. A comparative study of dilute VOCs treatment in a non-thermal plasma reactor. *Chem. Eng. J.* **2016**, *294*, 308–315. [[CrossRef](#)]
14. Li, S.; Dang, X.; Yu, X.; Abbas, G.; Zhang, Q.; Cao, L. The application of dielectric barrier discharge non-thermal plasma in VOCs abatement: A review. *Chem. Eng. J.* **2020**, *388*, 124275. [[CrossRef](#)]
15. Chung, W.-C.; Mei, D.-H.; Tu, X.; Chang, M.-B. Removal of VOCs from gas streams via plasma and catalysis. *Catal. Rev.* **2018**, *61*, 270–331. [[CrossRef](#)]
16. Berenguer, R.; Sieben, J.M.; Quijada, C.; Morallón, E. Electrocatalytic degradation of phenol on Pt- and Ru-doped Ti/SnO<sub>2</sub>-Sb anodes in an alkaline medium. *Appl. Catal. B Environ.* **2016**, *199*, 394–404. [[CrossRef](#)]
17. Xue, Z.-H.; Luan, D.; Zhang, H.; Lou, X.W. Single-atom catalysts for photocatalytic energy conversion. *Joule* **2022**, *6*, 92–133. [[CrossRef](#)]
18. Liu, Y.-H.; Fernández, C.A.; Varanasi, S.A.; Bui, N.N.; Song, L.; Hatzell, M.C. Prospects for Aerobic Photocatalytic Nitrogen Fixation. *ACS Energy Lett.* **2021**, *7*, 24–29. [[CrossRef](#)]
19. Liu, H.; Cheng, M.; Liu, Y.; Zhang, G.; Li, L.; Du, L.; Li, B.; Xiao, S.; Wang, G.; Yang, X. Modified UiO-66 as photocatalysts for boosting the carbon-neutral energy cycle and solving environmental remediation issues. *Coord. Chem. Rev.* **2022**, *458*, 214428. [[CrossRef](#)]
20. Poschl, U.; Shiraiwa, M. Multiphase chemistry at the atmosphere-biosphere interface influencing climate and public health in the anthropocene. *Chem. Rev.* **2015**, *115*, 4440–4475. [[CrossRef](#)]
21. Schultz, A.A.; Schauer, J.J.; Malecki, K.M. Allergic disease associations with regional and localized estimates of air pollution. *Environ. Res.* **2017**, *155*, 77–85. [[CrossRef](#)] [[PubMed](#)]
22. Gasana, J.; Dillikar, D.; Mendy, A.; Forno, E.; Ramos Vieira, E. Motor vehicle air pollution and asthma in children: A meta-analysis. *Environ. Res.* **2012**, *117*, 36–45. [[CrossRef](#)] [[PubMed](#)]
23. Suwannasual, U.; Lucero, J.; McDonald, J.D.; Lund, A.K. Exposure to traffic-generated air pollutants mediates alterations in brain microvascular integrity in wildtype mice on a high-fat diet. *Environ. Res.* **2018**, *160*, 449–461. [[CrossRef](#)] [[PubMed](#)]
24. Pikula, K.S.; Chernyshev, V.V.; Zakharenko, A.M.; Chaika, V.V.; Waissi, G.; Hai, L.H.; Hien, T.T.; Tsatsakis, A.M.; Golokhvast, K.S. Toxicity assessment of particulate matter emitted from different types of vehicles on marine microalgae. *Environ. Res.* **2019**, *179*, 108785. [[CrossRef](#)] [[PubMed](#)]
25. Zhang, Y.; Deng, W.; Hu, Q.; Wu, Z.; Yang, W.; Zhang, H.; Wang, Z.; Fang, Z.; Zhu, M.; Li, S.; et al. Comparison between idling and cruising gasoline vehicles in primary emissions and secondary organic aerosol formation during photochemical ageing. *Sci. Total Environ.* **2020**, *722*, 137934. [[CrossRef](#)]
26. Fanizza, C.; De Berardis, B.; Ietto, F.; Soggiu, M.E.; Schiro, R.; Inglessis, M.; Ferdinandi, M.; Incoronato, F. Analysis of major pollutants and physico-chemical characteristics of PM<sub>2.5</sub> at an urban site in Rome. *Sci. Total Environ.* **2018**, *616–617*, 1457–1468. [[CrossRef](#)]
27. Gorchov Negron, A.M.; McDonald, B.C.; McKeen, S.A.; Peischl, J.; Ahmadov, R.; de Gouw, J.A.; Frost, G.J.; Hastings, M.G.; Pollack, I.B.; Ryerson, T.B.; et al. Development of a Fuel-Based Oil and Gas Inventory of Nitrogen Oxides Emissions. *Environ. Sci. Technol.* **2018**, *52*, 10175–10185. [[CrossRef](#)]



28. Gholami, F.; Tomas, M.; Gholami, Z.; Vakili, M. Technologies for the nitrogen oxides reduction from flue gas: A review. *Sci. Total Environ.* **2020**, *714*, 136712. [[CrossRef](#)]
29. Liu, Z.; Yu, F.; Ma, C.; Dan, J.; Luo, J.; Dai, B. A Critical Review of Recent Progress and Perspective in Practical Denitration Application. *Catalysts* **2019**, *9*, 771. [[CrossRef](#)]
30. Hong, Z.; Wang, Z.; Li, X. Catalytic oxidation of nitric oxide (NO) over different catalysts: An overview. *Catal. Sci. Technol.* **2017**, *7*, 3440–3452. [[CrossRef](#)]
31. Jacobson, M.Z.; Seinfeld, J.H.; Carmichael, G.R.; Streets, D.G. The effect on photochemical smog of converting the U.S. fleet of gasoline vehicles to modern diesel vehicles. *Geophys. Res. Lett.* **2004**, *31*. [[CrossRef](#)]
32. Shi, Z.; Zhang, J.; Xiao, Z.; Lu, T.; Ren, X.; Wei, H. Effects of acid rain on plant growth: A meta-analysis. *J. Environ. Manag.* **2021**, *297*, 113213. [[CrossRef](#)] [[PubMed](#)]
33. Pignattelli, S.; Broccoli, A.; Piccardo, M.; Terlizzi, A.; Renzi, M. Effects of polyethylene terephthalate (PET) microplastics and acid rain on physiology and growth of *Lepidium sativum*. *Environ. Pollut.* **2021**, *282*, 116997. [[CrossRef](#)]
34. Marinos, R.E.; Campbell, J.L.; Driscoll, C.T.; Likens, G.E.; McDowell, W.H.; Rosi, E.J.; Rustad, L.E.; Bernhardt, E.S. Give and Take: A Watershed Acid Rain Mitigation Experiment Increases Baseflow Nitrogen Retention but Increases Stormflow Nitrogen Export. *Environ. Sci. Technol.* **2018**, *52*, 13155–13165. [[CrossRef](#)] [[PubMed](#)]
35. Feng, X.; Liu, Q.; Wang, S.; Cen, L.; Li, H. Arsenopyrite weathering in acid rain: Arsenic transfer and environmental implications. *J. Hazard. Mater.* **2021**, *420*, 126612. [[CrossRef](#)]
36. Lu, C.; Zhou, Q.; Wang, W.; Wei, S.; Wang, C. Freeze-thaw resistance of recycled aggregate concrete damaged by simulated acid rain. *J. Clean. Prod.* **2021**, *280*, 124396. [[CrossRef](#)]
37. Schirmer, W.N.; Olanyk, L.Z.; Guedes, C.L.B.; Quessada, T.P.; Ribeiro, C.B.; Capanema, M.A. Effects of air/fuel ratio on gas emissions in a small spark-ignited non-road engine operating with different gasoline/ethanol blends. *Environ. Sci. Pollut. Res. Int.* **2017**, *24*, 20354–20359. [[CrossRef](#)]
38. McGee Hargrove, M.; Snow, S.J.; Luebke, R.W.; Wood, C.E.; Krug, J.D.; Krantz, Q.T.; King, C.; Copeland, C.B.; McCullough, S.D.; Gowdy, K.M.; et al. Effects of Simulated Smog Atmospheres in Rodent Models of Metabolic and Immunologic Dysfunction. *Environ. Sci. Technol.* **2018**, *52*, 3062–3070. [[CrossRef](#)]
39. Lewis, A.C. The changing face of urban air pollution. *Science* **2018**, *359*, 744–745. [[CrossRef](#)]
40. Ali, Y.; Razi, M.; De Felice, F.; Sabir, M.; Petrillo, A. A VIKOR based approach for assessing the social, environmental and economic effects of “smog” on human health. *Sci. Total Environ.* **2019**, *650*, 2897–2905. [[CrossRef](#)]
41. Mahboob, I.; Shafiq, I.; Shafique, S.; Akhter, P.; Amjad, U.-e.-S.; Hussain, M.; Park, Y.-K. Effect of active species scavengers in photocatalytic desulfurization of hydrocracker diesel using mesoporous  $\text{Ag}_3\text{VO}_4$ . *Chem. Eng. J.* **2022**, *441*, 136063. [[CrossRef](#)]
42. Shafiq, I.; Hussain, M.; Shehzad, N.; Maaafa, I.M.; Akhter, P.; Amjad, U.-e.-s.; Shafique, S.; Razaq, A.; Yang, W.; Tahir, M.; et al. The effect of crystal facets and induced porosity on the performance of monoclinic  $\text{BiVO}_4$  for the enhanced visible-light driven photocatalytic abatement of methylene blue. *J. Environ. Chem. Eng.* **2019**, *7*, 103265. [[CrossRef](#)]
43. Guo, D.; Feng, D.; Zhang, Y.; Zhang, Y.; Zhao, Y.; Zhou, Z.; Sun, J.; Quan, C.; Chang, G.; Sun, S. Carbon material-TiO<sub>2</sub> for photocatalytic reduction of CO<sub>2</sub> and degradation of VOCs: A critical review. *Fuel Process. Technol.* **2022**, *231*, 107261. [[CrossRef](#)]
44. Fujishima, A.; Honda, K. Electrochemical photolysis of water at a semiconductor electrode. *Nature* **1972**, *238*, 37–38. [[CrossRef](#)]
45. Gao, X.; Huang, K.; Zhang, Z.; Meng, X. Bismuth chromate ( $\text{Cr}_2\text{Bi}_3\text{O}_{11}$ ): A new bismuth-based semiconductor with excellent photocatalytic activity. *Chem. Commun.* **2022**, *58*, 2014–2017. [[CrossRef](#)]
46. Meng, X.; Zhang, Z. Bismuth-based photocatalytic semiconductors: Introduction, challenges and possible approaches. *J. Mol. Catal. A Chem.* **2016**, *423*, 533–549. [[CrossRef](#)]
47. Liang, W.J.; Li, J.; Jin, Y.Q. Photocatalytic degradation of gaseous acetone, toluene, and p-xylene using a TiO<sub>2</sub> thin film. *J. Environ. Sci. Health Part A* **2010**, *45*, 1384–1390. [[CrossRef](#)]
48. Cao, L.; Gao, Z.; Suib, S.L.; Obee, T.N.; Hay, S.O.; Freihaut, J.D. Photocatalytic Oxidation of Toluene on Nanoscale TiO<sub>2</sub> Catalysts: Studies of Deactivation and Regeneration. *J. Catal.* **2000**, *196*, 253–261. [[CrossRef](#)]
49. Dong, F.; Guo, S.; Wang, H.; Li, X.; Wu, Z. Enhancement of the Visible Light Photocatalytic Activity of C-Doped TiO<sub>2</sub> Nanomaterials Prepared by a Green Synthetic Approach. *J. Phys. Chem. C* **2011**, *115*, 13285–13292. [[CrossRef](#)]
50. Li, J.-J.; Cai, S.-C.; Yu, E.-Q.; Weng, B.; Chen, X.; Chen, J.; Jia, H.-P.; Xu, Y.-J. Efficient infrared light promoted degradation of volatile organic compounds over photo-thermal responsive Pt-rGO-TiO<sub>2</sub> composites. *Appl. Catal. B Environ.* **2018**, *233*, 260–271. [[CrossRef](#)]
51. Li, F.B.; Li, X.Z.; Ao, C.H.; Lee, S.C.; Hou, M.F. Enhanced photocatalytic degradation of VOCs using Ln<sup>3+</sup>-TiO<sub>2</sub> catalysts for indoor air purification. *Chemosphere* **2005**, *59*, 787–800. [[CrossRef](#)] [[PubMed](#)]
52. Luu, C.L.; Nguyen, Q.T.; Ho, S.T. Synthesis and characterization of Fe-doped TiO<sub>2</sub> photocatalyst by the sol-gel method. *Adv. Nat. Sci. Nanosci. Nanotechnol.* **2010**, *1*, 015008. [[CrossRef](#)]
53. An, T.; Chen, J.; Nie, X.; Li, G.; Zhang, H.; Liu, X.; Zhao, H. Synthesis of carbon nanotube-anatase TiO(2) sub-micrometer-sized sphere composite photocatalyst for synergistic degradation of gaseous styrene. *ACS Appl. Mater. Interfaces* **2012**, *4*, 5988–5996. [[CrossRef](#)] [[PubMed](#)]
54. Li, Z.; Li, Z.; Zuo, C.; Fang, X. Application of Nanostructured TiO<sub>2</sub> in UV Photodetectors: A Review. *Adv. Mater.* **2022**, *34*, e2109083. [[CrossRef](#)] [[PubMed](#)]

55. Horváth, E.; Gabathuler, J.; Bourdieu, G.; Vidal-Revel, E.; Benthem Muñoz, M.; Gaal, M.; Grandjean, D.; Breider, F.; Rossi, L.; Sienkiewicz, A.; et al. Solar water purification with photocatalytic nanocomposite filter based on TiO<sub>2</sub> nanowires and carbon nanotubes. *npj Clean Water* **2022**, *5*, 10. [[CrossRef](#)]
56. Nawaz, M.; Miran, W.; Jang, J.; Lee, D.S. One-step hydrothermal synthesis of porous 3D reduced graphene oxide/TiO<sub>2</sub> aerogel for carbamazepine photodegradation in aqueous solution. *Appl. Catal. B Environ.* **2017**, *203*, 85–95. [[CrossRef](#)]
57. Zhang, J.-J.; Fang, S.-S.; Mei, J.-Y.; Zheng, G.-P.; Zheng, X.-C.; Guan, X.-X. High-efficiency removal of rhodamine B dye in water using g-C<sub>3</sub>N<sub>4</sub> and TiO<sub>2</sub> co-hybridized 3D graphene aerogel composites. *Sep. Purif. Technol.* **2018**, *194*, 96–103. [[CrossRef](#)]
58. Wang, T.; Shen, D.; Xu, T.; Jiang, R. Photocatalytic degradation properties of V-doped TiO<sub>2</sub> to automobile exhaust. *Sci. Total Environ.* **2017**, *586*, 347–354. [[CrossRef](#)]
59. Wang, J.; Asakura, Y.; Hasegawa, T.; Yin, S. High-concentration N-doped La<sub>2</sub>Ti<sub>2</sub>O<sub>7</sub> nanocrystals: Effects of nano-structuration and doping sites on enhancing the photocatalytic activity. *Chem. Eng. J.* **2021**, *423*, 130220. [[CrossRef](#)]
60. Pham, T.-D.; Lee, B.-K. Selective removal of polar VOCs by novel photocatalytic activity of metals co-doped TiO<sub>2</sub>/PU under visible light. *Chem. Eng. J.* **2017**, *307*, 63–73. [[CrossRef](#)]
61. Liu, X.; Gu, S.; Zhao, Y.; Zhou, G.; Li, W. BiVO<sub>4</sub>, Bi<sub>2</sub>WO<sub>6</sub> and Bi<sub>2</sub>MoO<sub>6</sub> photocatalysis: A brief review. *J. Mater. Sci. Technol.* **2020**, *56*, 45–68. [[CrossRef](#)]
62. Qian, X.; Yue, D.; Tian, Z.; Reng, M.; Zhu, Y.; Kan, M.; Zhang, T.; Zhao, Y. Carbon quantum dots decorated Bi<sub>2</sub>WO<sub>6</sub> nanocomposite with enhanced photocatalytic oxidation activity for VOCs. *Appl. Catal. B Environ.* **2016**, *193*, 16–21. [[CrossRef](#)]
63. Meng, X.; Zhang, Z. Bi<sub>2</sub>MoO<sub>6</sub> co-modified by reduced graphene oxide and palladium (Pd<sup>2+</sup> and Pd<sup>0</sup>) with enhanced photocatalytic decomposition of phenol. *Appl. Catal. B Environ.* **2017**, *209*, 383–393. [[CrossRef](#)]
64. Meng, X.; Li, Z.; Zeng, H.; Chen, J.; Zhang, Z. MoS<sub>2</sub> quantum dots-interspersed Bi<sub>2</sub>WO<sub>6</sub> heterostructures for visible light-induced detoxification and disinfection. *Appl. Catal. B Environ.* **2017**, *210*, 160–172. [[CrossRef](#)]
65. Zhou, H.; Wen, Z.; Liu, J.; Ke, J.; Duan, X.; Wang, S. Z-scheme plasmonic Ag decorated WO<sub>3</sub>/Bi<sub>2</sub>WO<sub>6</sub> hybrids for enhanced photocatalytic abatement of chlorinated-VOCs under solar light irradiation. *Appl. Catal. B Environ.* **2019**, *242*, 76–84. [[CrossRef](#)]
66. Lu, G.; Chu, F.; Huang, X.; Li, Y.; Liang, K.; Wang, G. Recent advances in Metal-Organic Frameworks-based materials for photocatalytic selective oxidation. *Coord. Chem. Rev.* **2022**, *450*, 214240. [[CrossRef](#)]
67. Yao, P.; Liu, H.; Wang, D.; Chen, J.; Li, G.; An, T. Enhanced visible-light photocatalytic activity to volatile organic compounds degradation and deactivation resistance mechanism of titania confined inside a metal-organic framework. *J. Colloid Interface Sci.* **2018**, *522*, 174–182. [[CrossRef](#)]
68. Qian, Y.; Zhang, F.; Pang, H. A Review of MOFs and Their Composites-Based Photocatalysts: Synthesis and Applications. *Adv. Funct. Mater.* **2021**, *31*, 2104231. [[CrossRef](#)]
69. Gelles, T.; Krishnamurthy, A.; Adebayo, B.; Rownaghi, A.; Rezaei, F. Abatement of gaseous volatile organic compounds: A material perspective. *Catal. Today* **2020**, *350*, 3–18. [[CrossRef](#)]
70. Liu, L.; Zhang, L.; Wang, F.; Qi, K.; Zhang, H.; Cui, X.; Zheng, W. Bi-metal-organic frameworks type II heterostructures for enhanced photocatalytic styrene oxidation. *Nanoscale* **2019**, *11*, 7554–7559. [[CrossRef](#)]
71. Zhang, Z.; Li, X.; Liu, B.; Zhao, Q.; Chen, G. Hexagonal microspindle of NH<sub>2</sub>-MIL-101(Fe) metal-organic frameworks with visible-light-induced photocatalytic activity for the degradation of toluene. *RSC Adv.* **2016**, *6*, 4289–4295. [[CrossRef](#)]
72. Rojas, S.; Garcia-Gonzalez, J.; Salcedo-Abraira, P.; Rincon, I.; Castells-Gil, J.; Padial, N.M.; Marti-Gastaldo, C.; Horcajada, P. Ti-based robust MOFs in the combined photocatalytic degradation of emerging organic contaminants. *Sci. Rep.* **2022**, *12*, 14513. [[CrossRef](#)]
73. Qian, Y.; Ma, D.; Zhong, J. Metal-Organic Frameworks With Variable Valence Metal-Photoactive Components: Emerging Platform for Volatile Organic Compounds Photocatalytic Degradation. *Front. Chem.* **2021**, *9*, 749839. [[CrossRef](#)] [[PubMed](#)]
74. Ding, M.; Cai, X.; Jiang, H.L. Improving MOF stability: Approaches and applications. *Chem. Sci.* **2019**, *10*, 10209–10230. [[CrossRef](#)] [[PubMed](#)]
75. Debono, O.; Hequet, V.; Le Coq, L.; Locoge, N.; Thevenet, F. VOC ternary mixture effect on ppb level photocatalytic oxidation: Removal kinetic, reaction intermediates and mineralization. *Appl. Catal. B Environ.* **2017**, *218*, 359–369. [[CrossRef](#)]
76. Jansson, I.; Kobayashi, K.; Hori, H.; Sánchez, B.; Ohtani, B.; Suárez, S. Decahedral anatase titania particles immobilized on zeolitic materials for photocatalytic degradation of VOC. *Catal. Today* **2017**, *287*, 22–29. [[CrossRef](#)]
77. Abidi, M.; Hajjaji, A.; Bouzaza, A.; Lamaa, L.; Peruchon, L.; Brochier, C.; Rtimi, S.; Wolbert, D.; Bessais, B.; Assadi, A.A. Modeling of indoor air treatment using an innovative photocatalytic luminous textile: Reactor compactness and mass transfer enhancement. *Chem. Eng. J.* **2022**, *430*, 132636. [[CrossRef](#)]
78. Abou Saoud, W.; Kane, A.; Le Cann, P.; Gerard, A.; Lamaa, L.; Peruchon, L.; Brochier, C.; Bouzaza, A.; Wolbert, D.; Assadi, A.A. Innovative photocatalytic reactor for the degradation of VOCs and microorganism under simulated indoor air conditions: Cu-Ag/TiO<sub>2</sub>-based optical fibers at a pilot scale. *Chem. Eng. J.* **2021**, *411*, 128622. [[CrossRef](#)]
79. Debono, O.; Gaudion, V.; Redon, N.; Locoge, N.; Thevenet, F. Photocatalytic treatment of VOC industrial emissions: IPA removal using a sensor-instrumented reactor. *Chem. Eng. J.* **2018**, *353*, 394–409. [[CrossRef](#)]
80. Gérardin, F.; Cloteaux, A.; Simard, J.; Favre, É. A photodriven energy efficient membrane process for trace VOC removal from air: First step to a smart approach. *Chem. Eng. J.* **2021**, *419*, 129566. [[CrossRef](#)]
81. Lyu, J.; Zhou, L.; Shao, J.; Zhou, Z.; Gao, J.; Li, J.; Dong, Y.; Wang, Z. Synthesis of TiO<sub>2</sub>/H<sub>2</sub>Ti<sub>3</sub>O<sub>7</sub> composite with nanoscale spiny hollow hierarchical structure for photocatalytic mineralization of VOCs. *Chem. Eng. J.* **2020**, *400*, 125927. [[CrossRef](#)]

82. Mothes, F.; Boge, O.; Herrmann, H. A chamber study on the reactions of O<sub>3</sub>, NO, NO<sub>2</sub> and selected VOCs with a photocatalytically active cementitious coating material. *Environ. Sci. Pollut. Res. Int.* **2016**, *23*, 15250–15261. [[CrossRef](#)] [[PubMed](#)]
83. Toma, F.L.; Bertrand, G.; Klein, D.; Coddet, C. Photocatalytic removal of nitrogen oxides via titanium dioxide. *Environ. Chem. Lett.* **2004**, *2*, 117–121. [[CrossRef](#)]
84. Kotzias, D.; Binas, V.; Kiriakidis, G. Smart Surfaces: Photocatalytic Degradation of Priority Pollutants on TiO<sub>2</sub>-Based Coatings in Indoor and Outdoor Environments-Principles and Mechanisms. *Materials* **2022**, *15*, 402. [[CrossRef](#)] [[PubMed](#)]
85. Ma, Y.; Li, L.; Wang, H.; Wang, W.; Zheng, K.; Guo, Q. Laboratory Study on Performance Evaluation and Automobile Exhaust Degradation of Nano-TiO<sub>2</sub> Particles-Modified Asphalt Materials. *Adv. Mater. Sci. Eng.* **2021**, *2021*, 5574013. [[CrossRef](#)]
86. Mahy, J.G.; Paez, C.A.; Hollevoet, J.; Courard, L.; Boonen, E.; Lambert, S.D. Durable photocatalytic thin coatings for road applications. *Constr. Build. Mater.* **2019**, *215*, 422–434. [[CrossRef](#)]
87. Yu, H.; Dai, W.; Qian, G.; Gong, X.; Zhou, D.; Li, X.; Zhou, X. The NO<sub>x</sub> Degradation Performance of Nano-TiO<sub>2</sub> Coating for Asphalt Pavement. *Nanomaterials* **2020**, *10*, 897. [[CrossRef](#)]
88. Singh, H.; Thind, P.S.; Singh, S.; John, S. Applicability of TiO<sub>2</sub>-Laden Asphalt Pavements in Reducing the Vehicular Pollution of Chandigarh, India. *CLEAN—Soil Air Water* **2022**, *50*, 2000461. [[CrossRef](#)]
89. Wang, D.; Leng, Z.; Hüben, M.; Oeser, M.; Steinauer, B. Photocatalytic pavements with epoxy-bonded TiO<sub>2</sub>-containing spreading material. *Constr. Build. Mater.* **2016**, *107*, 44–51. [[CrossRef](#)]
90. Livraghi, S.; Paganini, M.C.; Giamello, E.; Selloni, A.; Di Valentin, C.; Pacchioni, G. Origin of photoactivity of nitrogen-doped titanium dioxide under visible light. *J. Am. Chem. Soc.* **2006**, *128*, 15666–15671. [[CrossRef](#)]
91. Lee, H.U.; Lee, S.C.; Choi, S.; Son, B.; Lee, S.M.; Kim, H.J.; Lee, J. Efficient visible-light induced photocatalysis on nanoporous nitrogen-doped titanium dioxide catalysts. *Chem. Eng. J.* **2013**, *228*, 756–764. [[CrossRef](#)]
92. Hu, Z.; Xu, T.; Liu, P.; Oeser, M. Developed photocatalytic asphalt mixture of open graded friction course for degrading vehicle exhaust. *J. Clean. Prod.* **2021**, *279*, 123453. [[CrossRef](#)]
93. Lei, J.; Zheng, N.; Luo, F.; He, Y. Purification of automobile exhaust gas by activated carbon supported Fe<sup>3+</sup> modified nano-TiO<sub>2</sub> and its application on asphalt pavement. *Road Mater. Pavement Des.* **2020**, *22*, 2424–2440. [[CrossRef](#)]
94. Zhang, L.; Lu, Q.; Shan, R.; Zhang, F.; Muhammad, Y.; Huang, K. Photocatalytic degradation of vehicular exhaust by nitrogen-doped titanium dioxide modified pavement material. *Transp. Res. Part D Transp. Environ.* **2021**, *91*, 102690. [[CrossRef](#)]
95. Brattich, E.; Barbano, F.; Pulvirenti, B.; Pilla, F.; Bacchetti, M.; Di Sabatino, S. The effect of photocatalytic coatings on NO<sub>x</sub> concentrations in real-world street canyons. *Build. Environ.* **2021**, *205*, 108312. [[CrossRef](#)]
96. Qian, X.; Ren, M.; Yue, D.; Zhu, Y.; Han, Y.; Bian, Z.; Zhao, Y. Mesoporous TiO<sub>2</sub> films coated on carbon foam based on waste polyurethane for enhanced photocatalytic oxidation of VOCs. *Appl. Catal. B Environ.* **2017**, *212*, 1–6. [[CrossRef](#)]
97. Lorencik, S.; Yu, Q.L.; Brouwers, H.J.H. Photocatalytic coating for indoor air purification: Synergetic effect of photocatalyst dosage and silica modification. *Chem. Eng. J.* **2016**, *306*, 942–952. [[CrossRef](#)]
98. Sansotera, M.; Geran Malek Kheyli, S.; Baggioli, A.; Bianchi, C.L.; Pedefferri, M.P.; Diamanti, M.V.; Navarrini, W. Absorption and photocatalytic degradation of VOCs by perfluorinated ionomeric coating with TiO<sub>2</sub> nanopowders for air purification. *Chem. Eng. J.* **2019**, *361*, 885–896. [[CrossRef](#)]
99. Rosset, A.; Bartolomei, V.; Laisney, J.; Shandilya, N.; Voisin, H.; Morin, J.; Michaud-Soret, I.; Capron, I.; Wortham, H.; Brochard, G.; et al. Towards the development of safer by design TiO<sub>2</sub>-based photocatalytic paint: Impacts and performances. *Environ. Sci. Nano* **2021**, *8*, 758–772. [[CrossRef](#)]
100. Morin, J.; Gandolfo, A.; Temime-Roussel, B.; Strekowski, R.; Brochard, G.; Bergé, V.; Gligorovski, S.; Wortham, H. Application of a mineral binder to reduce VOC emissions from indoor photocatalytic paints. *Build. Environ.* **2019**, *156*, 225–232. [[CrossRef](#)]
101. Fernandez-Catala, J.; Berenguer-Murcia, A.; Cazorla-Amoros, D. Photocatalytic Oxidation of VOCs in Gas Phase Using Capillary Microreactors with Commercial TiO<sub>2</sub> (P25) Fillings. *Materials* **2018**, *11*, 1149. [[CrossRef](#)] [[PubMed](#)]
102. Damyar, N.; Khavanin, A.; Jafari, A.J.; Mahabadi, H.A.; Mirzaei, R.; Ghomi, H.; Mousavi, S.M. Removal of sulfur dioxide from air using a packed-bed DBD plasma reactor (PBR) and in-plasma catalysis (IPC) hybrid system. *Environ. Sci. Pollut. Res. Int.* **2021**, *28*, 42821–42836. [[CrossRef](#)] [[PubMed](#)]
103. Poulakis, E.; Philippopoulos, C. Photocatalytic treatment of automotive exhaust emissions. *Chem. Eng. J.* **2017**, *309*, 178–186. [[CrossRef](#)]
104. Ola, O.; Maroto-Valer, M.M. Synthesis, characterization and visible light photocatalytic activity of metal based TiO<sub>2</sub> monoliths for CO<sub>2</sub> reduction. *Chem. Eng. J.* **2016**, *283*, 1244–1253. [[CrossRef](#)]
105. Pellegrino, F.; Zangirolami, M.; Minero, C.; Maurino, V. Portable photoreactor for on-site measurement of the activity of photocatalytic surfaces. *Catal. Today* **2020**, *340*, 363–368. [[CrossRef](#)]
106. Héquet, V.; Raillard, C.; Debono, O.; Thévenet, F.; Locoge, N.; Le Coq, L. Photocatalytic oxidation of VOCs at ppb level using a closed-loop reactor: The mixture effect. *Appl. Catal. B Environ.* **2018**, *226*, 473–486. [[CrossRef](#)]
107. Bellè, U.; Invernizzi, M.; Polvara, E.; Lucotti, A.; Diamanti, M.V.; Sironi, S.; Pedefferri, M. A novel nanotubular TiO<sub>2</sub>-based Plug-Flow reactor for gas phase photocatalytic degradation of toluene. *Chem. Eng. J.* **2022**, *437*, 135323. [[CrossRef](#)]

108. Gao, W.; Zhang, X.; Su, X.; Wang, F.; Liu, Z.; Liu, B.; Zhan, J.; Liu, H.; Sang, Y. Construction of bimetallic Pd-Ag enhanced AgBr/TiO<sub>2</sub> hierarchical nanostructured photocatalytic hybrid capillary tubes and devices for continuous photocatalytic degradation of VOCs. *Chem. Eng. J.* **2018**, *346*, 77–84. [[CrossRef](#)]
109. Zhao, J.; Ren, G.; Li, Z.; Meng, X. Design and experimental analysis of a novel slant-plate photoreactor. *AIChE J.* **2022**, e17883. [[CrossRef](#)]